Article:
Speak, TH, Medeiros, DJ, Blitz, MA et al. (1 more author) (2021) OH Kinetics with a Range of Nitrogen-Containing Compounds: N-Methylformamide, t-Butylamine, and N-Methyl-propane Diamine. The Journal of Physical Chemistry A. ISSN 1089-5639

https://doi.org/10.1021/acs.jpca.1c08104

OH Kinetics with a Range of Nitrogen Containing Compounds: N-Methylformamide; *t*-Butylamine and N-Methyl-propane diamine

Thomas H. Speak[1], Diogo J. Medeiros[1], Mark A. Blitz[1,2,*] and Paul W. Seakins[1,*]

1 - School of Chemistry, University of Leeds, Leeds, LS2 9JT, UK

2 - National Centre for Atmospheric Science (NCAS), University of Leeds, Leeds, LS2 9JT, UK

Abstract

Emissions of amines and amides to the atmosphere are significant from both anthropogenic and natural sources and amides can be formed as secondary pollutants. Relatively little kinetic data exist on overall rate coefficients with OH, the most important tropospheric oxidant and even less on site specific data which control the product distribution. Structure activity relationships (SAR) can be used to estimate both quantities. Rate coefficients for the reaction of OH with *t*-butylamine (k_1), N-methyl-1,3-propanediamine (k_2) and N-methylformamide (k_3) have been measured using laser flash photolysis coupled with laser induced fluorescence. Proton transfer mass spectrometry (PTR-MS) has been used to ensure the reliable introduction of these low vapour pressure N-containing compounds and to give qualitative information on products. Supporting *ab initio* calculations are presented for the *t*-butylamine system.

The following rate coefficients have been determined:

$$k_{1,\,298K} = (1.66 \pm 0.20) \times 10^{-11}\ \text{cm}^3\ \text{molecule}^{-1}\ \text{s}^{-1}$$

$$k(T)_1 = 1.65 \times 10^{-11}\ (T/300)^{-0.69}\ \text{cm}^3\ \text{molecule}^{-1}\ \text{s}^{-1}$$

$$k_{2,\,293\,K} = (7.09 \pm 0.22) \times 10^{-11}\ \text{cm}^3\ \text{molecule}^{-1}\ \text{s}^{-1}$$

$$k_{3,298K} = (1.03 \pm 0.23) \times 10^{-11}\ \text{cm}^3\ \text{molecule}^{-1}\ \text{s}^{-1}$$

For OH + *t*-butylamine *ab initio* calculations predict that the fraction of N-H abstraction is 0.87. The dominance of this channel was qualitatively confirmed by end-product analysis. The reaction of OH with N-methyl-1,3-propanediamine also had a negative temperature dependence, but the reduction in rate coefficient was complicated by reagent loss. The measured rate coefficient for reaction 3 is in good agreement with a recent relative rate study.

The results of this work and literature data are compared with recent structure activity relationship estimates for the reaction of OH with reduced nitrogen compounds. Whilst the SARs reproduce the overall rate coefficients for reactions, site specific agreement with this work and other literature is less strong.

1.0 Introduction

Nitrogen-containing compounds have received significant interest in recent years as they have the ability to reversibly complex with carbon dioxide, CO_2. This makes carbon capture and storage (CCS) possible with N-compounds, in particular with low vapour pressure amines, e.g. ethanol amine.[1-3] Previously, we have studied a range of such compounds in terms of their reactivity towards OH in order to provide knowledge of their kinetics and the breakdown mechanism of these compounds if released into the atmosphere.[4-8]

The atmospheric concentration of amines are controlled by physical uptake into droplets or on to surfaces or by reaction with the OH radical. The rate coefficients for the reaction of OH with various amines ranges from ~1 – 10 x 10^{-11} cm^3 $molecule^{-1}$ s^{-1}. The corresponding lifetimes with respect to removal by OH range from <1 to ~6 hr for a typical daytime [OH] of 5 x 10^6 molecule cm^{-3}. Techniques have been developed to measure both point emissions[9] and ambient concentrations[10]. Given the short lifetimes and variability of the sources, there are wide variations in ambient amine concentrations as discussed by Mao et al.[11] who reported values of 2 – 20 and 5 – 50 pptv for C_1 and C_2 methylamines.

A particular problem with oxidation of amines in the atmosphere is that OH abstraction at the N-H bond leads to N-centred radicals, which are generally unreactive toward oxygen such that reaction with NOx is possible to form carcinogenic nitrosamines and nitramines. Therefore, it is important to know not only the overall rate of reaction with OH, but also site-specific rate coefficients for reaction with N-H.

Whilst the potential use of amines in CCS has triggered recent interest in nitrogen containing species, amines and amides can be emitted or produced in a range of processes.[12-14] The role of these compounds in aerosol formation or in the production of highly toxic nitrosamines, nitramines and isocyanates means that there is a need to determine kinetic data for these compounds as input to atmospheric[15] or combustion models.[16] In the absence of easily attainable data, structure activity relationships (SAR) can provide estimations of both overall and site-specific rate coefficients. Recently, a structure activity relationship (SAR) has been proposed for reduced nitrogen compounds,[17] and the measurements of the range of nitrogen compounds in this work (*t*-butylamine, N-methyl-1,3-propanediamine and N-methylformamide) provide a good test of this SAR and an earlier SAR proposed by Nielsen et al.[3]

The properties of amines and amides generate a range of practical problems, from the handling of low vapour pressure compounds to the mixing basic compounds with OH precursors, which are typically acidic. This paper explores these kinetic problems with the use of our recently developed high pressure and temperature apparatus.[18-19]

In this study, the reaction of OH with *t*-butylamine, *t*-$C_4H_9NH_2$, is investigated as while previously it has been shown to form *t*-butyl nitramine,[20] the yield of the N-centred radical was not assigned.

$$OH + t\text{-}C_4H_9NH_2 \xrightarrow{k_{1a}} H_2O + t\text{-}C_4H_9NH \qquad \text{R1a}$$

$$OH + t\text{-}C_4H_9NH_2 \xrightarrow{k_{1b}} H_2O + t\text{-}C_4H_8NH_2 \quad \text{R1b}$$

Diamines, e.g. piperazine, have a higher potential (on a molar basis) for CO_2 capture. The ring compound, piperazine has been the subject of several studies[7, 21], and in this work we extend the database on diamines to include the previous unstudied diamine N-methyl-1,3-propanediamine ($H_2NCH_2CH_2CH_2NHCH_3$):

$$OH + H_2NCH_2CH_2CH_2NHCH_3 \xrightarrow{k_2} H_2O + \text{products} \quad \text{R2}$$

Another potential problem of studying the gas-phase oxidation of N-compounds is aerosol formation.[22] As basic species they can undergo reaction with acids, which leads to particle growth in the atmosphere. N-methyl-1,3-propanediamine, the most basic compound investigated in this study, visibly undergoes an acid-base reaction when exposed to moist air. For this reason, PTR-MS was used to ensure that the diamine reached a stable level in the reaction cell.

Following abstraction from a C-H bond by OH, atmospheric oxidation of amines can form amides;[17] our understanding regarding lifetimes and fate in the atmosphere of these compounds is limited due to the small number of previous studies.[13, 23-26] The third reaction studied in this work is that of OH with N-methylformamide:

$$OH + CH_3\text{-}NH\text{-}CHO \xrightarrow{k_{3a}} H_2O + CH_3\text{-}NH\text{-}CO \quad \text{R3a}$$

$$OH + CH_3\text{-}NH\text{-}CHO \xrightarrow{k_{3b}} H_2O + CH_2\text{-}NH\text{-}CHO \quad \text{R3b}$$

$$OH + CH_3\text{-}NH\text{-}CHO \xrightarrow{k_{3c}} H_2O + CH_3\text{-}N\text{-}CHO \quad \text{R3c}$$

The lack of datasets is in part due to the low-vapour pressure of amides which makes the generation of reliable and sufficient concentrations for pseudo-first order kinetic studies difficult. For example, the vapour pressure of N-methylformamide, CH_3-NH-CHO, is less than 0.5 Torr at 298 K, and as in our previous study on monoethanol amine,[4] reproducible delivery of the reagent to the reactor is a challenge. In this study, a proton-transfer-reaction time-of-flight mass spectrometer (PTR-MS) was used to monitor the delivery of the CH_3-NH-CHO to the reaction cell and identify the products of its reaction with OH, in the presence of O_2. The study of amides and particularly formamides, is important due to the potential for forming highly toxic isocyanates.

2.0 Experimental

The apparatus has recently been described in detail, except the coupling of the PTR-MS to the reactor gas in order to sample the exhaust gas.[18-19] In brief, a 248 nm excimer laser (KrF, Lambda Physik 205) operating at 0.2 – 10 Hz was used to photolyse the OH precursor ($(CH_3)_3COOH$ or H_2O_2). The photolysis laser illuminated the majority of reactor, which is a 2 cm internal diameter stainless-steel tube about 50 cm in length, lined with an internal quartz

tube. This tube can be heated along its length, and at the end, gas was sampled by a pinhole, 500 μm, into a low-pressure expansion cell where the hydroxyl radical (OH) was detected by laser induced fluorescence (LIF). Only a minority of the gas was sampled, the remainder was slowly exhausted downstream, where a needle valve was located and adjusted to set the reactor pressure, typically 1500 Torr. Temperatures were measured using both thermocouples located near the pinhole, but also by calibration with the well-characterised temperature dependence of the OH + CH_4 reaction.[18, 27]

Gases were delivered to the reactor using mass flow controllers (Tylan and Brooks) with nitrogen buffer gas as the main flow. The OH precursor was either hydrogen peroxide (H_2O_2) or tertiary butyl hydroperoxide (*t*-C_4H_9OOH) and these were delivered to the reactor via a pressurized bubbler situated before the mass flow controller (MFC). *t*-C_4H_9OOH has a higher vapour pressure than H_2O_2 and can pass through the MFC unaffected, so *t*-C_4H_9OOH only required a flow of 100s SCCM, while the H_2O_2 required up to 2 SLM to achieve a suitable OH signal. N-methylformamide and N-methyl-1,3-propanediamine were also delivered to the reactor with bubblers located before the mass flow controller. *t*-butylamine had sufficient vapour pressure that it could be reliably added to a cylinder and pressurised with N_2. The OH precursor bubblers were sufficiently pressurized (~3 bar) so that the mass flow controller was operational. The bubblers for the N-compounds had pressure gauges attached in order to determine the pressure, set by a regulator, and a thermometer located on the outside measured the bubbler temperature. Overall, the total flow was maintained to be ca. 10 SLM. A pressure gauge (10000 Torr MKS) was suitably located to measure the pressure in the reactor.

Nitrogen (generated from scrubbing air with an O_2 trap) was used for the main bath gas and to pressurize the OH precursor bubbler. As these flows were constant for any particular experiment, any OH removal with the impurities would have been constant and not affected our kinetic assignment when the N-compound was added. Tests indicated that the nitrogen contained a residual, few 10^{15} molecule cm^{-3} of O_2. For the N-compound bubblers, cylinder oxygen free nitrogen was used (BOC, 5-20 ppm O_2 present) to ensure only the N-compound and nitrogen was further added to the reactor. In some experiments O_2 (BOC, 99.9% purity) was added via an extra mass flow controller. Merck supplied N-methylformamide (> 98.5%), and N-methyl-1,3-propanediamine (98%), were placed in the bubbler for a few hours to ensure all O_2 was removed. The bubbler was a 500 mL screw top glass bottle (Duran), where a modified aluminum cone coupled the screw top to the bottle to maintain a gas-tight seal and allow gases to flow in and out.

The 248 nm photolysis (5-50 mJ cm^{-2} $pulse^{-1}$) of either hydrogen peroxide (Merck, 30 wt% in H_2O, but gradually concentrated in the bubbler) or *t*-butyl hydroperoxide (Merck, 70 wt% in H_2O) generated the hydroxyl radical:

$$H_2O_2/t\text{-}C_4H_9OOH \xrightarrow{248\ \mathrm{nm}} OH \qquad \text{(P1,P2)}$$

The typical [t-C_4H_9OOH] was ~1 x 10^{15} molecule cm^{-3} and with a laser fluence of 25 mJ cm^{-2} $pulse^{-1}$ and an absorption cross section of 2 x 10^{-20} cm^2 at 248 nm (with unit quantum yield for OH production)[28], the initial [OH] is estimated to have been ~5 x 10^{11} molecule cm^{-3}. The

minimum cross-section of the photolysis volume was 1 cm^2, which guaranteed that gas within a few mm of the pinhole is illuminated. At the flow rate through the cell, roughly every 1 mm from the pinhole represents ca. 6 milliseconds. Therefore, the OH traces are described by only chemistry rather than a combination of chemistry and transport. The gas sampled through the pinhole experiences supersonic jet expansion, where the rapid expansion means that the chemistry is frozen and is a proxy for the chemistry in the high-pressure reactor. The transport time is typically ~20 μs, which limits the fastest measurable kinetics, but pseudo-first-order rate coefficients up to 50000 s^{-1} can be measured without any distortion in the exponential decay.[18] The fidelity of the kinetics is maintained as long as the OH is probed within the jet, which is between 1 -2 cm as long the expansion cell is pumped to below 1 Torr using the rotary pump backing a supercharger. The dye laser ((SL4000 using Rhodamine 6G dye and pumped at 532 nm by a Spectron, YAG -SL803), tuned to the strongest OH transition at ca. 282 nm (($A^2\Sigma$ (v′ = 1) ← X $^2\Pi$(v′′=0))), entered the gas expansion cell in the plane and at right angles to the reactor flow, so that is was close to the pinhole without hitting it (which produces a large scattering signal). At right angles to the probe laser, the OH fluorescence light passed through a 308 nm filter (Materion) before being imaged using a biconvex lens onto the photomultiplier (CPM, Perkin Elmer, 1943). The signal from the photomultiplier was displayed and integrated on the oscilloscope (LeCroy Wave-runner LT354) before being passed to the PC for storage. A LabVIEW program was used to control the firing of the photolysis and probe lasers via a delay generator (BNC 555). Typically, 200 time delays were used to build-up the OH trace, where this time scan was repeated several times to improve the quality. An example trace can be found in the inset to Figure 1.

Concentrations were arranged such that [N-compound]>>[OH] and therefore the OH was controlled by pseudo-first-order kinetics:

$$[OH]_t = [OH]_0 \times \exp(-k't) \quad \text{(E1)}$$

where k' is the pseudo-first-order rate coefficient given by:

$$k' = k_{bi}[\text{N-compound}] + k_d \quad \text{(E2)}$$

Here k_{bi} is the relevant bimolecular rate coefficient and k_d represents the additional combined first order (diffusional) and pseudo-first order (reaction with precursor/carrier gas impurities) rate coefficient. A plot of k' *vs* [N-compound] (e.g. Figure 1) yields k_{bi} as the gradient and k_d as the intercept. However, a major challenge in the study of these compounds is ensuring that a stable concentration of the N-compound has been obtained. In these experiments, the N-compounds and certain products were monitored by a proton transfer time-of-flight mass spectrometer (PTR-MS, Kore). The PTR-MS is designed to sample gas at or close to atmospheric pressure. Attaching a pipe (1/4”) to the exit side of the needle valve allowed the reactor gas to be directed towards the PTR-MS. A valve inside the PTR-MS was adjusted so that this pressurized reactor gas was sampled under the correct conditions. Details of the masses sampled are given in the relevant results section.

A number of experiments for *t*-butylamine were carried out using a conventional slow flow laser flash photolysis cell at lower pressures (21 and 51 Torr) of nitrogen. Full details on the apparatus can be found in Onel et al.[4] or Baez-Romero et al.[29]

3.0 Results and Discussion

3.1 OH + t-butylamine, t-$C_4H_9NH_2$

3.1.1 Overall rate coefficient

The vapor pressure of *t*-butylamine is sufficiently high that its concentration can be accurately determined using pressure gauges. In addition, its stability means that it can reliably be stored in either glass bulbs or cylinders. Experiments on reaction (1):

$$OH + t\text{-}C_4H_9NH_2 \xrightarrow{k_1} H_2O + C_4H_{10}N \qquad (R1)$$

carried out over multiple days showed little variation in the observed OH and *t*-butylamine rate coefficient assigned at room temperature (293-300 K). Rate coefficient measurements were carried out over a range of temperatures, 293 – 500 K, summarized in Table 1. An example bimolecular plot from these experiments is shown in Figure 1.

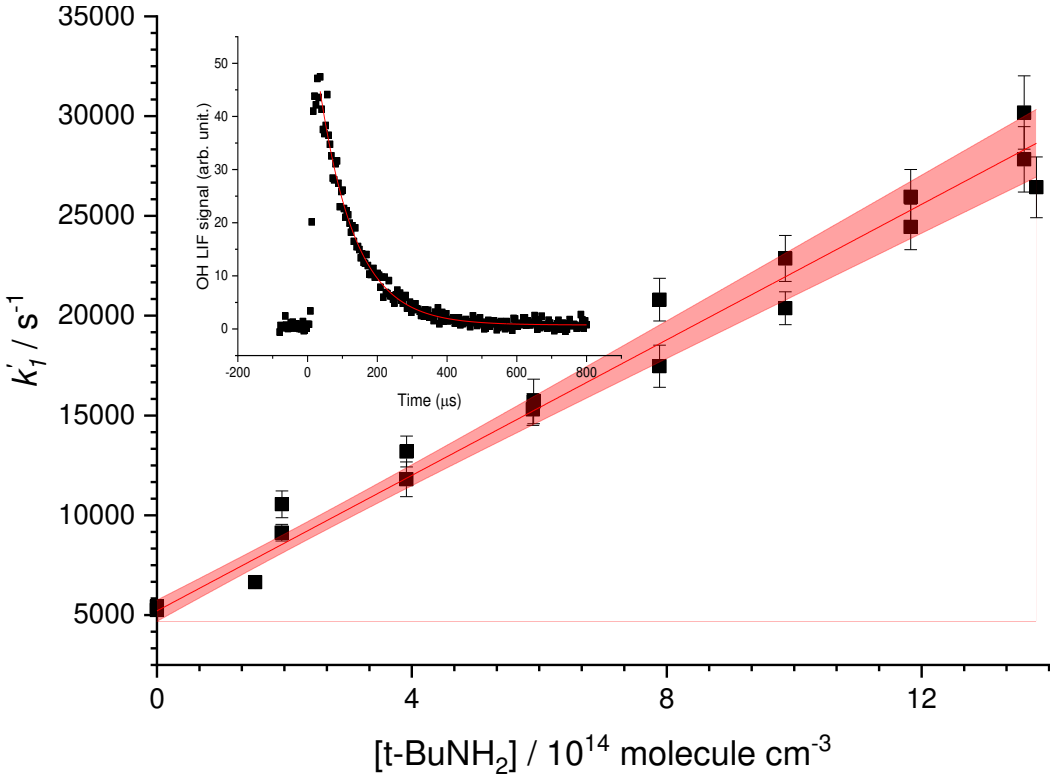

Figure 1. An example OH and *t*-butylamine, (*t*-$BuNH_2$) bimolecular plot used to generate k_1 at 303 K, 1478 Torr with *t*-C_4H_9OOH as the OH precursor, $k_{1,\ OH+tBuNH2}$ = (1.69 ± 0.07) × 10^{-11} cm^3 $molecule^{-1}$ s^{-1}. Inset is an example OH fluorescence decay trace, used to generate the point at 1.5 × 10^{14} molecule cm^{-3} $tBuNH_2$ on the bimolecular plot. The vertical bars represent the statistical error from the fits to the exponential decays and the 95% confidence interval is shown as the shaded area.

Table 1 shows the rate coefficients for *t*-butylamine and OH measured both in the high-pressure reactor and in a conventional low-pressure cell. Two OH precursors were used, *t*-C_4H_9OOH and H_2O_2. It is clear that where H_2O_2 was used, a lower rate coefficient was assigned.

Table 1. Summary of experimental results as a function of temperature and precursor

Precursor	*T* (K)	*P* (Torr)	10^{11} k_1 /cm^3 molecule^{-1} s^{-1}	Precursor	*T* (K)	P (Torr)	10^{11} k_1 /cm^3 molecule^{-1} s^{-1}
H_2O_2	291	1371	1.30 ± 0.02	H_2O_2	357 ± 8	1251	1.39 ± 0.02
H_2O_2	293	1250	1.27 ± 0.03	H_2O_2	427 ± 15	1253	1.40 ± 0.02
H_2O_2	293	1287	1.36 ± 0.03	H_2O_2	483 ± 21	1488	1.36 ± 0.03
H_2O_2	295	1297	1.29 ± 0.03	H_2O_2	485 ± 21	1270	1.42 ± 0.05
t-butOOH	293	1350	1.69 ± 0.11	*t*-butOOH	297	1377	1.67 ± 0.04
t-butOOH	295	1260	1.70 ± 0.07	*t*-butOOH	303	1478	1.69 ± 0.07
t-butOOH	298	21	1.60 ± 0.05	*t*-butOOH	350 ± 5	51	1.43 ± 0.05
t-butOOH	298	21	1.66 ± 0.05	*t*-butOOH	400 ± 10	51	1.52 ± 0.08
t-butOOH	298	21	1.54 ± 0.07	*t*-butOOH	450 ± 15	51	1.22 ± 0.06
t-butOOH	298	21	1.63 ± 0.07	*t*-butOOH	500 ± 20	51	1.12 ± 0.05
t-butOOH	298	21	1.80 ± 0.10				

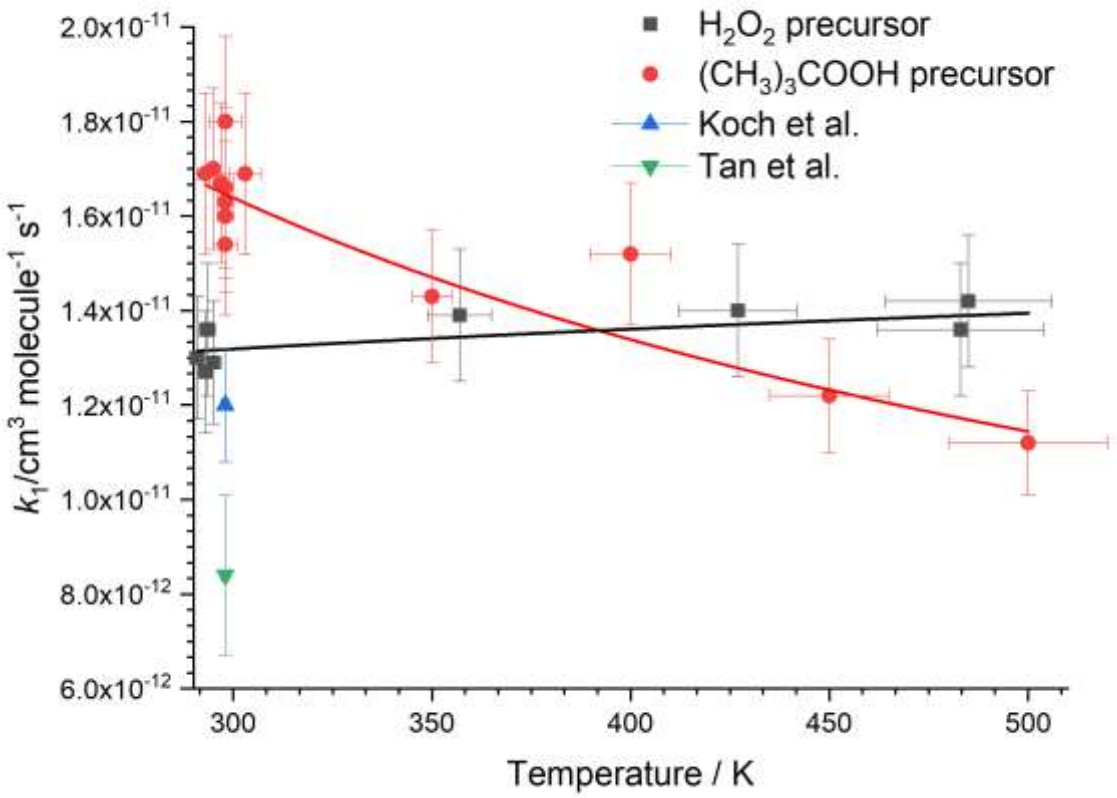

Figure 2. The observed temperature dependence of OH and *t*-butylamine (R1) where OHwas generated via the photolysis of either H_2O_2 (black points and line) or *t*-C_4H_9OOH (red points and line).From Table 1 and Figure 2, it is evident that the rate coefficients show a small but significant difference with the two OH precursors. This effect is assigned to reaction between the more acidic H_2O_2 with the basic *t*-butylamine. This effect was even more dramatic for the more basic N-methyl-propane diamine, see below. The addition of the much more acidic Cl

atom precursor oxalyl chloride, $(ClCO)_2$, to the reaction cell, resulted in the complete removal of the N-compounds.

A reduction of up to 35 % in the m/z 74 (t-$C_4H_9NH_2$-H^+) was observed on the PTR-MS in the presence of H_2O_2 in the gas flow. This effect was presumably caused by the aforementioned acid-base reaction as the sample time post reactor before sampling by the PTR-MS is significant. For this reason, the peak area could not be used to reliably correct the *in situ* concentrations of *t*-butylamine in the presence of H_2O_2. On the other hand, when t-C_4H_9OOH was added to the flow, no measurable decrease was observed in the peak at m/z 74. Therefore, the faster rate coefficient at room temperature with the less acidic t-C_4H_9OOH precursor is our preferred measurement. In addition, the significant negative temperature dependence of the rate coefficient is more consistent with previous studies on OH/amine reactions[4-5, 8, 30-31] and with our reaction rate theory calculation, see Section 3.1.2 The calculated potential energy surface does not predict the slight positive temperature dependence for the rate coefficient that is indicated when H_2O_2 is the precursor, see Figure 2.

We therefore recommend the values obtained with the t-C_4H_9OOH precursor. An average of the room temperature measurements obtained from both reaction cells (Table 1) gives: $k_{1,\ OH+tBuNH2}$ = (1.66 ± 0.15) × 10^{-11} cm^3 $molecule^{-1}$ s^{-1}, the error is 2σ of the room temperature measurements. The temperature dependence of the reaction of OH with *t*-butylamine is given by: $k_{1,OH+tBuNH2}(T)$= 1.65 × 10^{-11} $(T/300)^{-0.69}$ cm^3 $molecule^{-1}$ s^{-1}.

The rate coefficient at room temperature has been measured previously: Koch et al.[32] assigned $k_{1,\ OH+tBuNH2}$ = (1.20 ± 0.12) × 10^{-11} cm^3 $molecule^{-1}$ s^{-1} using flash photolysis-resonance fluorescence technique in a non-conventional approach and Tan et al.[20] assigned k_1 = (0.84 ± 0.17) × 10^{-11} cm^3 $molecule^{-1}$ s^{-1} using a relative rate technique.

The result of the Koch et al. study agrees more closely with this study, although the error bars of the two determinations do not quite overlap. Although *t*-butylamine is significantly easier to handle than many other amines, it is possible that systematic reagent handling issues (e.g. absorption of reagent onto storage vessel or delivery line walls) could account for the difference between the two studies. Radical-radical reactions can also interfere with flash photolysis studies, especially if the species in excess absorbs significantly at the photolysis wavelengths. Such secondary chemistry can both enhance, or reduce OH loss. At 248 nm, the photolysis wavelength of this work, the expected absorption cross-section of a primary amine is expected to be below 1 x 10^{-19} cm^2 and therefore at the laser energies and *t*-butylamine concentrations used in this study, it is impossible to generate the radical concentrations required to compete with OH loss rates of ~20000 s^{-1}. Koch et al. used 193 nm flash photolysis and this is expected to produce more significant photolysis of the amine.

Tan et al. noted the issues in the delivery of *t*-butylamine, highlighting additional loss processes through reaction of the amine with both the OH precursors and walls, and emphasized that a systematic error in accounting for the non-OH losses of the amine could have influenced their results.

3.1.2 Theoretical calculations

In terms of products, the reaction of OH with *t*-butylamine is relatively simple as there are only two possible H atom abstraction sites, either from the CH_3 or the NH_2:

$$OH + (CH_3)_3CNH_2 \xrightarrow{k_{1a}} (CH_3)_3CNH + H_2O \qquad \text{(R1a)}$$

$$OH + (CH_3)_3CNH_2 \xrightarrow{k_{1b}} (CH_3)_2CH_2CNH_2 + H_2O \qquad \text{(R1b)}$$

In the study by Tan et al.[20] the potential energy surface (PES) for abstraction from *t*-butylamine by OH was calculated. The authors identified a pre-reactive complex located before transition-states to form the products of either C-H or N-H abstraction sites. We have reproduced the *ab initio* results of Tan et al. by carrying out calculations at the CCSD(T)/CBS//mp2/6-311++g(3df,3pd) and CCSD(T)/CBS//M06-2X/6-311++g(3df,3pd) levels of theory. The turning points of the PES are given in Figure 3. Master Equation analysis was carried out on this PES using the Master Equation solver MESMER.[33] Forward rate coefficients from the pre-reactive complex to the products were calculated using the RRKM option in MESMER. In our analysis, transition-states (TS) to products were adjusted in unison via a non-linear least-squares regression, until a good match between modelled rate-coefficients (extracted via a Bartis-Widom analysis[34]) and the experimental values generated with the *t*-C_4H_9OOH precursor was obtained (see Table 1). Adjusting the TS in unison maintains the *ab initio* energy gap of 2.5 kJ mol^{-1}, which is expected to be relatively correct.[35]

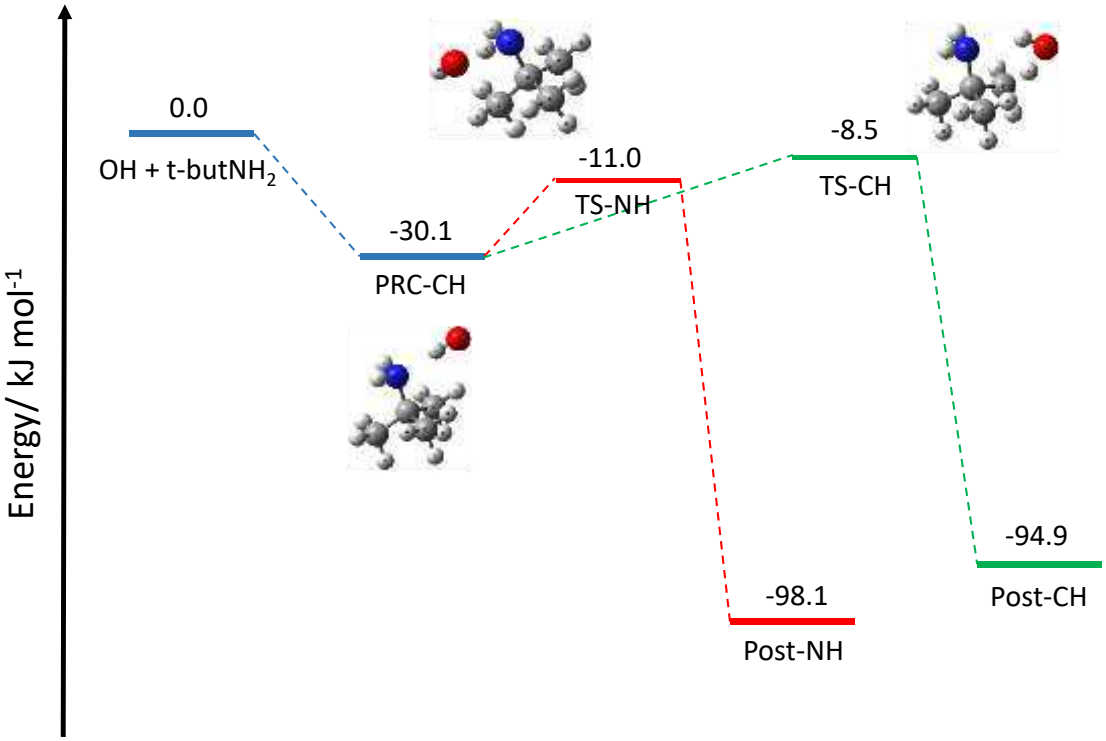

Figure 3. PES for the reaction between OH and *t*-butylamine calculated at the CCSD(T)/CBS//mp2/6-311++g(3df,3pd) level of theory. The pre-reactive complex, PRC-CH, is common to both product channels. The *ab initio* energies for TS-NH and TS-CH are equal to -6.38 and -3.88 kJ mol^{-1}, respectively, the values shown in the figure are the results of the data-fitting.

Table 2. Parameters for k_1 and the PES for Reaction 1 and literature values for k_1

	MESMER		
ILT, A_{ILT}	2.20×10^{-11} cm^3 molecule^{-1} s^{-1}		
n_{ILT}, $(T/298)^n$	0.34		
TS-NH	-11.0 kJ mol^{-1}		
$k_1 = A_1 (T/300)^n$	Leeds	Koch et al.	Tan et al.
10^{12} A_1 / cm^3 molecule^{-1} s^{-1}	16.5 ± 0.01	12.0 ± 1.2	8.4 ± 1.7
n_1	-0.69 ± 0.02		
$k_{1,NH}/k_1$	0.87		

An excellent fit to the experimental data was obtained by adjusting the kinetic parameters for PRC-CH formation, A_{ILT} and n_{ILT}, and the transition-states for the abstractions, adjusted in unison, as previously described. (TS-NH is 2.5 kJ mol^{-1} below the C-H abstraction, TS-CH). These fitting parameters are given in Table 2. The MESMER-assigned transition-state TS-NH is ca. 5 kJ mol^{-1} lower than the *ab initio* value, which is within the uncertainty of the *ab initio* calculation, assuming that the rate coefficients are accurate. We use the results obtained with the less acidic precursor *t*-C_4H_9OOH as an attempt to reduce the interference from the acid-base reaction, but particularly as the temperature is increased, this interference might become important.

From this MESMER fitting, based on the *ab initio* calculations, it was observed that N-H abstraction is the dominant channel, $\frac{k_{1a}}{k_1} = 0.87$. This result is essentially independent of temperature. In addition, as the energy gap between the N-H and C-H transition states was maintained to the calculated *ab initio* value, this abstraction branching ratio is essentially independent of the fitted value of TS-NH. Therefore, it is most likely that reaction R1a is dominant.

The product of R1b is expected to react with O_2 and form OH at low pressures (R4a) where the chemically activated peroxy species, $(CH_3)_3CH_2O_2CNH_2$*, can undergo an internal rearrangement to produce OH. At higher pressures, collisional deactivation of $(CH_3)_3CH_2O_2CNH_2$* will produce the stabilized peroxy radical (R4b):

$$(CH_3)_3CH_2CNH_2 + O_2 \xrightarrow{k_4} \text{Products} \qquad \text{(R4)}$$

$$(CH_3)_3CH_2CNH_2 + O_2 \xrightarrow{k_{4a}} (CH_3)_2NH + CH_2O + OH \qquad \text{(R4a)}$$

$$\xrightarrow{k_{4b}} (CH_3)_3CH_2O_2CNH_2 \qquad \text{(R4b)}$$

Ab initio calculations were carried out ((CCSD(T)/CBS//MP2/6-311++g(3df,3pd) and CCSD(T)/CBS//M062X/6-311++g(3df,3pd)) to determine the PES for reaction R4 (see Figure S1 in the SI), and MESMER calculations on this PES indicated that OH would be significantly recycled (30%) at 500 K and 1500 Torr. Further experiments were carried out in a low-pressure (~20 - 50 Torr) apparatus (promoting reaction R4a over R4b), on OH and *t*-butylamine, where O_2 was added to the system. Under all conditions, no significant OH recycling was observed,

although under similar conditions OH recycling has been observed for both amines[6-8] and aldehydes.[36-37] This result is consistent with the low abstraction branching ratio for R1b of 0.13.

Tan et al.[20] calculated a similar branching ratio (0.96, CCSD(T)-F12//MP2 calculations, 0.80, CCSD(T)-F12//M06-2X calculations) favoring N-H abstraction. In addition, they observed a negligible difference in rate coefficient between $C_4H_9NH_2$ and $C_4D_9NH_2$ (KIE = 0.97 ± 0.03) which they took as evidence that abstraction was occurring predominantly at the NH_2 group.

3.1.3 End product analysis

In this work, PTR-MS was used to investigate the products of reaction R1; significant peaks were observed following photolysis at m/z 30, 57, 58, 59 a.u., where H_2O_2 was the OH precursor. H_2O_2 was selected for the product investigation over *t*-C_4H_9OOH due to the complex mass spectra generated when *t*-C_4H_9OOH was used, hence giving a simplified product assignment. When experiments were carried out under NOx free conditions the only stable product observed from the amino abstraction is through the formation of propan-2-imine (observed at m/z 58 ($C_3H_8N^+$)), via fragmentation of the amino radical in the reaction chamber (analogous to t-butoxy decomposition to methyl radicals and acetone[38]). As there is always a significant [O_2] (≥10^{15} molecule cm^{-3}), the radical formed via the minor (0.13) abstraction of a methyl C-H, R1b, is going to react at high pressures via R4b to form its peroxy radical, which is likely to form stable molecules via self-reaction.

Additional experiments were carried out where a small concentration of NO_2 ($4 \times 10^{12} – 5 \times 10^{13}$ molecule cm^{-3}) was added to the flow of gases; [NO_2] was greater than the [OH] but not in great excess. The presence of NO_2 should convert the $(CH_3)_3CNH$ radicals (product of R1a) to the nitramine via reaction R5:

$$(CH_3)_3CNH + NO_2 \xrightarrow{k_5} (CH_3)_3CHNNO_2 \qquad \text{(R5)}$$

where $(CH_3)_3CHNNO_2$ is *t*-butyl nitramine, a stable compound. The PTR-MS observed the formation of $(CH_3)_3CHNNO_2$ via its protonated parent mass at m/z 119 ($(CH_3)_3CHNNO_2$-H^+), see Figure 4.

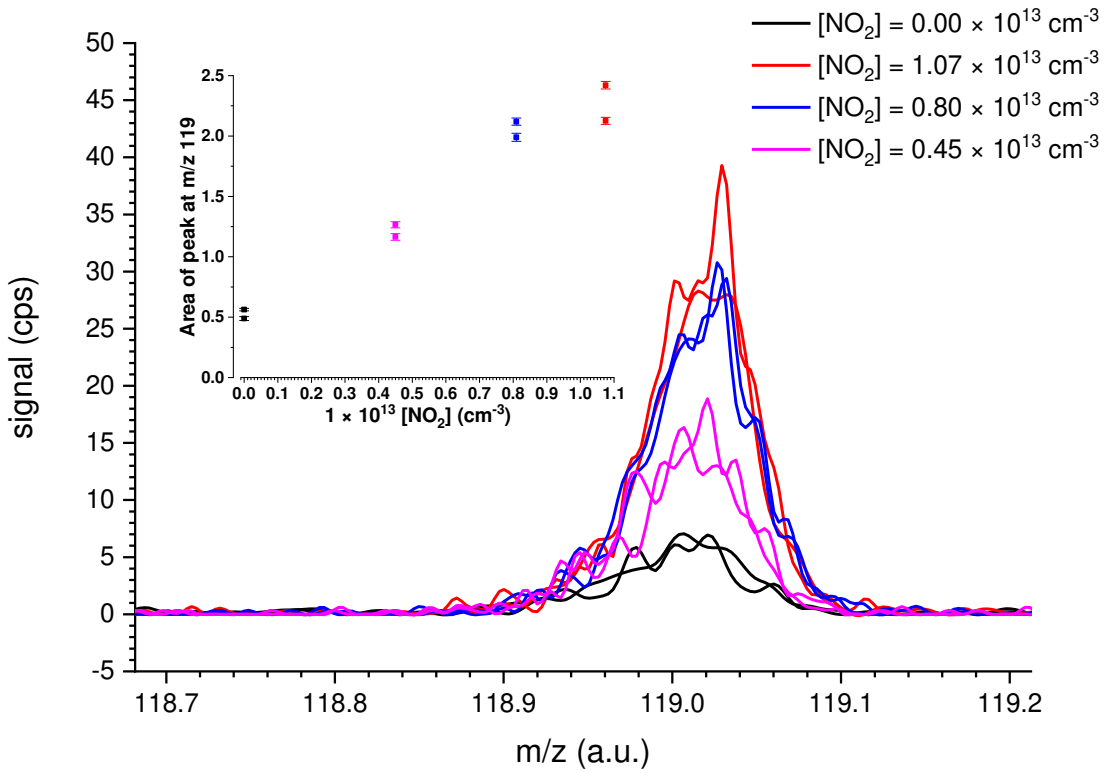

Figure 4. Formation of the nitramine $(CH_3)_3CHNNO_2$ at mass m/z 119 from the reaction between OH and *t*-butylamine in the presence of a small amount of NO_2, i.e. R1a followed by R4. This is a difference spectrum, where any signal in the absence of OH precursor has been subtracted.

From Figure 4, it can be seen that the m/z 119 signal is increasing with added NO_2, which is wholly consistent with R5 being in competition with other loss processes for $(CH_3)_3CNH$ such as decomposition and self-reaction. The rate coefficient for R5 has been determined by Lazarou et al.[39] at ~1 x 10^{-12} cm^3 $molecule^{-1}$ s^{-1} so that pseudo-first order rate coefficient for reaction R5 will only be of the order of 5 – 10 s^{-1} which is likely to be smaller or comparable to the self-reaction.

There were other lower mass signals (m/z 57, 91) that were observed to increase upon the addition of NO_2, but only the m/z 119 signal can be uniquely assigned as nitramine formation, $(CH_3)_3CHNNO_2$. In the study by Tan et al.,[20] it was concluded that *t*-butyl nitramine is formed via reactions R1 and R5. They also observed the signal at m/z 119 and noted that the parent mass partially fragmented to the *t*-butyl ion at m/z 57.

In the absence of added NO_2, no definite product assignments from R1 could be made from the PTR-MS. The fate of the amino radical, $(CH_3)_3CNH$, the major channel of R1, is uncertain as it exhibits little or no reactivity towards O_2. Although the addition of NO_2 to the system identifies the amino radical by titrating it to the stable molecule, *t*-butyl nitramine, R5, quantitation of the product yields from the reaction of OH with *t*-butylamine, R1, is presently beyond the scope of this work.

3.2 N-methyl-1,3-propanediamine, $H_2NCH_2CH_2CH_2NHCH_3$

N-methyl-1,3-propanediamine ($H_2NCH_2CH_2CH_2NHCH_3$) is an example of a compound that is both difficult to handle and deliver to the reaction cell. Due to its high CO_2 solubility and fast reaction rate, the use of this compound in carbon capture and storage techniques has earned increased attention.[40-41] This diamine is colourless, but significant contact with air turns it yellow. Attempts to transfer it a cylinder for pressured delivery proved futile and a bubbler was used to store and deliver the diamine. The slight problem of using H_2O_2 as the OH precursor when studying *t*-butylamine was much worse for the diamine. The PTR-MS showed that the diamine signal - parent mass peak at m/z 89 (88+1) - was completely removed when H_2O_2 was added to the reaction cell.

This result was reinforced by observing that the bimolecular plot showed no increase in the removal rate constant with added diamine. Meaningful bimolecular plots were possible with *t*-C_4H_9OOH as the OH precursor, but there was some reaction between the reagents before the reactor as evidenced by the PTR-MS. The best compromise was to add the minimum amount of hydroperoxide in order to have a workable OH signal. Our guide that diamine was being reliably delivered was the linearity of the bimolecular plot. The results for reaction R2

$$OH + H_2NCH_2CH_2CH_2NHCH_3 \xrightarrow{k_2} H_2O + C_4H_{11}N_2 \qquad (R2)$$

are summarized in the Table 3 and Figure 5 shows an example of a kinetic trace and the resultant bimolecular plot.

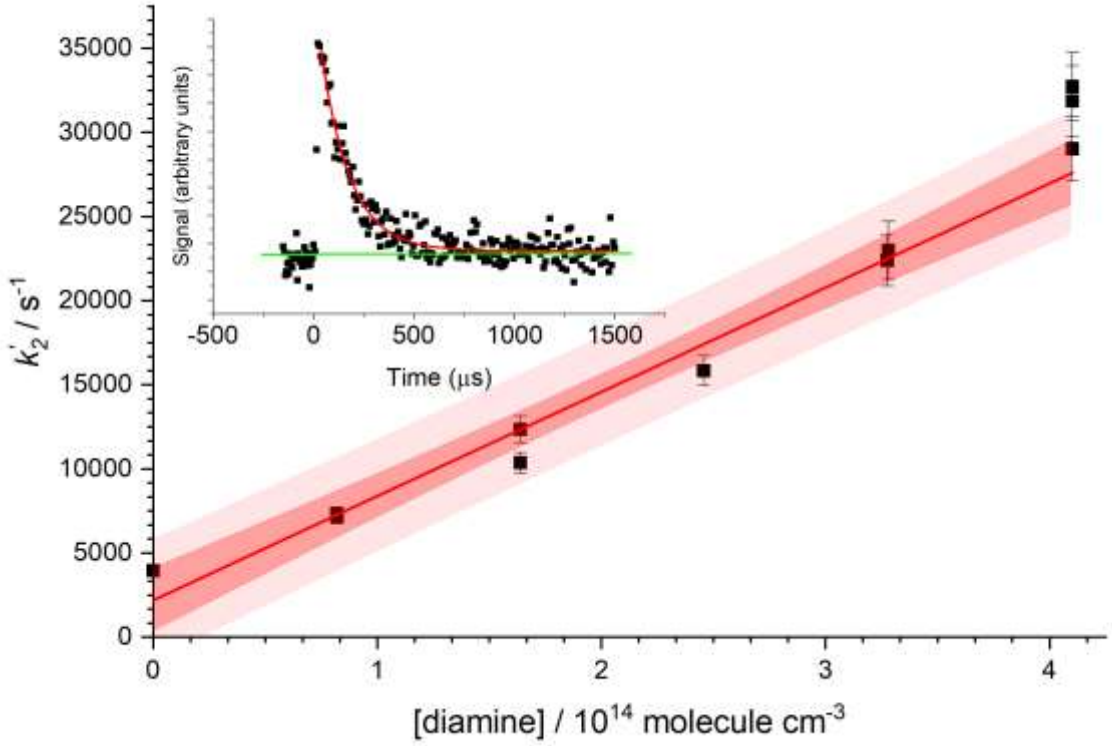

Figure 5. An example of a bimolecular plot for diamine delivered by a bubbler using *t*-C_4H_9OOH as the OH precursor at 353 K. The inset is representative of the quality of the OH kinetic traces. The shaded areas give the 1 and 2σ confidence limits.

Table 3. The rate coefficients collected for N-methyl propane diamine and OH using *t*-C_4H_9OOH as the precursor.

Temperature (K)	$10^{11}k_2$ /cm^3 molecule^{-1} s^{-1}	Pressure (Torr)	Temperature (K)	$10^{11}k_2$ /cm^3 molecule^{-1} s^{-1})	Pressure (Torr)
293	7.07 ± 0.32	1500 ± 30	353	6.86 ± 0.29	1608 ± 30
293	6.54 ± 0.27	1550 ± 30	421	4.40 ± 0.22	1610 ± 30
293	7.60 ± 0.52	1610 ± 30	432	2.38 ± 0.18	1370 ± 30
293	7.16 ± 0.08	1550 ± 30	489	2.20 ± 0.16	1600 ± 30
353	7.61 ± 0.20	1596 ± 30	496	1.38 ± 0.22	1380 ± 30
353	6.20 ± 0.33	1600 ± 30			

From Table 3, it can be seen that the bimolecular rate coefficient between OH and diamine is fast. An average of the room temperature data gives: $k_{2,\ OH+diamine,293K}$ = (7.09 ± 0.22) × 10^{-11} cm^3 molecule^{-1} s^{-1}. In fact, the true rate coefficient for this reaction is potentially even faster as some diamine removal was observed in the presence of *t*-C_4H_9OOH. Therefore, the actual diamine concentration at the observation point is somewhat lower than our calculated value, however, it is difficult to quantify the loss. Every C and N site in diamine has a different H, so potentially there are six possible reaction channels. The fact that diamine reacts faster with OH than N-methylformamide and *t*-butylamine is most probably a result of the weaker bonds in diamine. From Table 3, it appears that the reaction rate coefficient exhibits a very significant negative temperature dependence. However, the temperature effect is probably not entirely chemical and results from the acidic peroxide removing a larger amount of the basic diamine by the time it has reached the reaction zone, i.e. the volume within a few mm of the sampling pinhole.

This reaction between OH and diamine is a curio as it serves as an example of the limits of doing gas-phase kinetics. Studying this diamine has proven challenging, as it is not only difficult to handle and deliver on its own, but it is also removed in the presence of the OH precursors.

3.3 OH + N-methylformamide

As discussed in the introduction, a significant source of uncertainty in the kinetic measurements for N-methylformamide (MF) was the error associated with defining the

concentration of the reagent in the reactor. For MF, the vapour pressure was insufficient at 290 - 300 K [42] (< 0.5 Torr) to allow accurate concentrations to be assigned to gas mixtures.[4] MF was added via the 'bubbler' method, where the ambient vapour above liquid MF was sampled by a backing flow of nitrogen. Delivered concentrations of MF were calculated from the Antoine equation log(P/bar) = A - [B/(*T*/K + C)], using values of A = 4.99796, B = 2134.031, C = -45.071[43] and these were measured over the range 369.6 - 472.4 K. The time taken to reach a stable concentration of added MF was notably slow, typically an hour, where the PTR-MS was used to monitor and determine when the MF was fully delivered. The concentration of MF was monitored at m/z 61 ([$HCONHCH_3$]H+) and its carbon 13 isotope peak at m/z 62.

For these experiments, H_2O_2 was used as the OH precursor. No problems were observed for this this acidic precursor, unlike for the other N-compounds. The OH concentration was between $1 – 10 \times 10^{12}$ molecule cm^{-3}, so its removal in the presence of much higher [MF] ($1 – 10 \times 10^{14}$ molecule cm^{-3}):

$$OH + CH_3NHCHO \xrightarrow{k_3} H_2O + C_2H_4NO \qquad \text{(R3)}$$

was pseudo-first-order and the OH time trace was a single exponential (see inset to Figure 6). Examples of typical bimolecular plots are shown in Figure 6, the different intercepts are a result of different [H_2O_2]. This result plus the literature values are summarized in Table 4. Kinetic determinations at room temperature were made by averaging 10 bimolecular plots, temperature (293 – 300 K), and from which the room temperature bimolecular rate coefficient $k_{3,\,OH+MF}$ was assigned as $(1.03 \pm 0.23) \times 10^{-11}$ cm^3 $molecule^{-1}$ s^{-1}, where errors are given as 2σ.

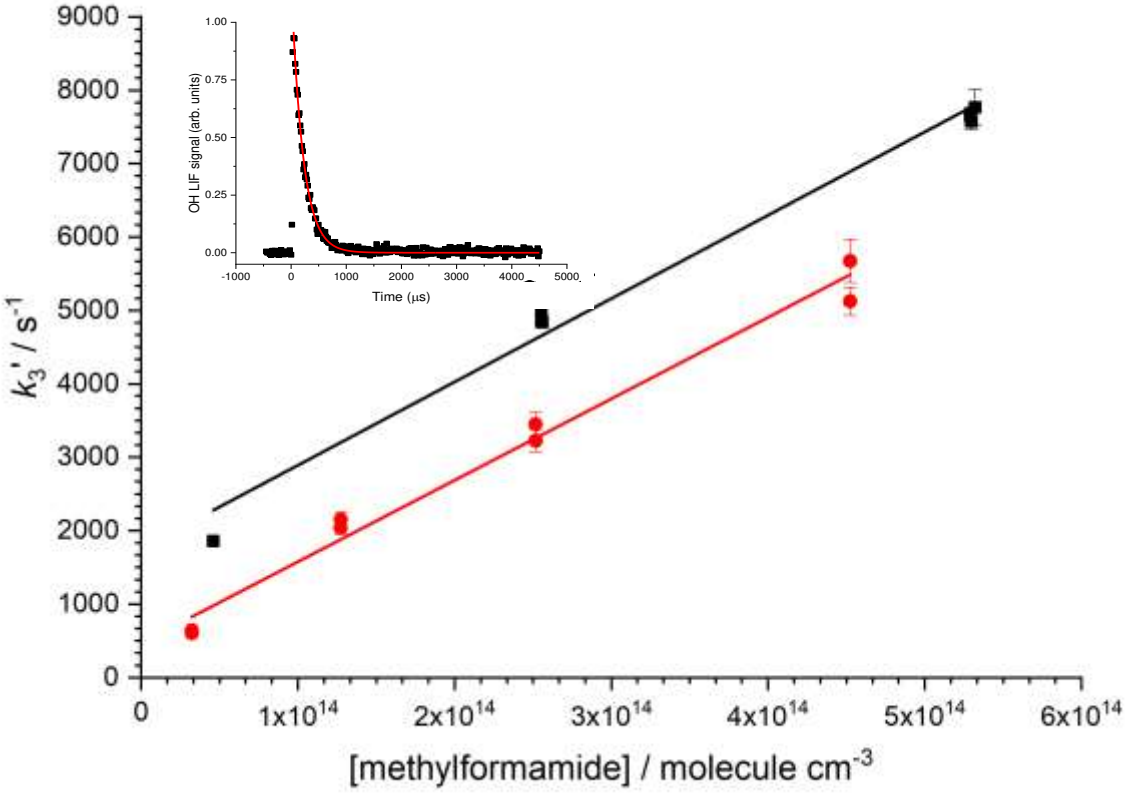

Figure 6. Two example bimolecular plots for OH + N-methylformamide, MF (R3) at different precursor (H_2O_2) concentrations. The gradients of the plots are: (1.14 ± 0.12) × 10^{-11} cm^3 molecule^{-1} s^{-1} (black line) and (1.11 ± 0.10) × 10^{-11} cm^3 molecule^{-1} s^{-1} (red line), with errors given are statistical at the 2σ level. The inset shows a typical pseudo-first order decay of OH.

Table 4. Rate coefficient for OH + N-methylformamide (MF)

Reference	Technique	10^{12} $k_{3,OH+MF}$ /cm^3 molecule^{-1} s^{-1}
This Study	Laser flash photolysis/laser induced fluorescence	10.3 ± 2.3
Solignac et al. [24]	Relative rate	8.6 ± 2.0
Borduas et al. [25]	Relative rate	10.1 ± 0.6
Bunkan et al. [26]	Laser flash photolysis/laser induced fluorescence	5.7 ± 1.7

From Table 4, it can be seen that our rate coefficient is in excellent agreement with the recent relative rate study by Borduas et al., [25] where a PTR-MS was used to track the loss of the N-methylformamide. The relative rate study by Solignac et al.[24] used FTIR spectroscopy to monitor N-methylformamide, and their result is lower but within the errors of the present study. The direct time-resolved study by Bunkan et al.[26] measured k_3 almost a factor of two lower than this study. It is possible that their low rate coefficient might be a consequence of not establishing that the N-methylformamide was fully delivered.

Reaction R3 has the possibility of abstraction of an H from three potential sites (k_{3a}, k_{3b}, k_{3c}), as depicted in scheme S1:

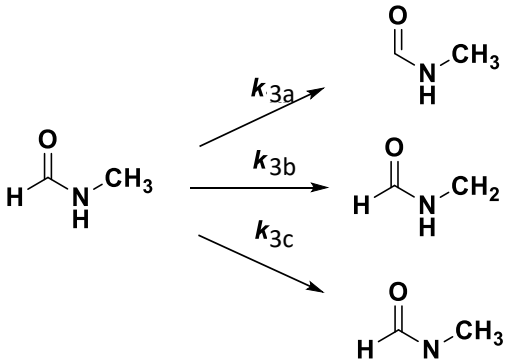

Scheme 1: Potential abstraction sites in the reaction of OH with N-methylformamide.

In both the studies by Borduas et al. and Bunkan et al., theoretical calculations were carried out and it was noted that the barrier for N-H abstraction (channel 3c) is too high to contribute to the reaction at room temperature. The barriers for formyl and methyl C—H abstractions were calculated to be similar and the abstractions were assigned equal probability, 50:50; this ratio is very sensitive to these abstraction energies, so small energy differences can change this ratio significantly. The stable product of formyl C—H abstraction is expected to be methyl isocyanate[20] (R3a followed by R6) and in the study by Barnes et al.[13] this product was observed with a yield estimated to be ≤ 30 %.

$$OH + CH_3\text{-}NH\text{-}CHO \xrightarrow{k_{3a}} H_2O + CH_3\text{-}NH\text{-}CO \qquad \text{R3a}$$

$$CH_3\text{-}NH\text{-}CO + O_2 \rightarrow CH_3NCO + HO_2 \qquad \text{R6}$$

The expected first generation product of the methyl C—H abstraction is formylformamide, $NH(CHO)_2$ and this was observed with ~50% yield by Barnes et al. In the more recent study by Bunkan et al., the methyl isocyanate and formylformamide yields were assigned 65% and 16%, respectively, where a PTR TOFMS monitored the products and the assumption of equal sensitivity for detection was made. The study by Barnes et al.[13] used FTIR to detect and assign the product yields. Reference spectra were not available to Barnes et al. and the ~50% yield is based on analogies with product studies in the reaction of OH with formamide.

Attempts were made in this study to detect the products (with added O_2) using PTR-TOFMS and the peak at m/z 76 (a.u.), which is consistent with methyl isocyanate (MIC, 57+19). A large

peak at m/z 74 was present when the excimer laser was fired at 5 Hz, but was much reduced when the repetition rate was lowered to 1 Hz; this peak can be assigned to protonated formyl formamide (FF, 73+1). This repetition rate dependence indicates that the products of the reaction could be photolysed at 248 nm, with secondary chemistry leading to product formation. Uncalibrated comparison of the increase in peak area at m/z 74 and m/z 76 at 1 Hz leads to a ratio of 0.59(±0.02):0.41(±0.02) formyl formamide to methyl isocyanate. However, this ratio is not quantitative, being subject to a large uncertainty on the response factor for methyl isocyanate and to the source of formylformamide as either a primary or secondary reaction product.

When PTR-MS measurements were made with lower water concentrations, increases were observed at both m/z 58 (MIC-H^+) and 76 (MIC-H_3O^+) at 1 Hz, with a peak at m/z 74 only becoming apparent at higher (3, 5 Hz) repetition rates. Therefore, it was concluded that quantitative product analysis was not possible for this system. The theoretical calculations of Borduas et al. [25] indicated that the radical formed via formyl C—H abstraction in the presence of O_2 forms methyl isocyanate and HO_2, and so is in agreement with earlier studies. However, the methyl C—H abstraction radical reactions with O_2 is mostly likely to form the peroxy radical, HCO-NH-CH_2O_2 under our high-pressure conditions. In this case, formylformamide is presumably the result of the self-reaction of this peroxy radical. However, the origin of the signal of formylformamide was uncertain.

4.0 Conclusions and Comparison with SAR

The kinetics of the reactions of OH with n-butylamine, N-methyl-1,3-propanediamine and N-methylformamide have been determined using a flash-photolysis/OH laser-induced-fluorescence technique. These N-compounds present a range of handling and delivery challenges. A PTR-MS coupled to the exhaust of the reactor was able to indicate that the compound was fully delivered in the case of the low-vapor pressure N-methylformamide. The PTR-MS measurements also showed that the diamine and the OH precursor *t*-C_4H_9OOH did not react significantly. *t*-butylamine was the most straight*t*-forward compound to determine its kinetics with OH, and by comparing these results to reaction rate theory it was determined that the reaction proceeded predominantly via N-H abstraction to form the N-centered radical, $(CH_3)_3CNH$. Qualitative experimental support for dominance of N-H abstraction comes from the absence of any products associated with C-H abstraction and the lack of any observed OH recycling that would be expected from the chemically activated peroxy radical, $(CH_3)_3CH_2O_2CNH_2$*, that would be formed following C-H abstraction.

The OH + amine rate coefficients measured in this work are compared to selected other nitrogen containing compounds in Table 5. The overall rate coefficient for the reaction of OH with *t*-butylamine is lower than other amines. As might be expected from the lack of α-CH bonds, the rate coefficient for C-H abstraction, $k_{1,C\text{-}H} = 2.2 \times 10^{-12}$ cm^3 molecule^{-1} s^{-1}, is small, comparable to OH abstractions from other molecules with *t*-butyl groups (e.g. OH + *t*-C_4H_9OH ~9×10^{-13} cm^3 molecule^{-1} s^{-1} [44], OH + *t*-C_4H_9OOH 3.6×10^{-12} cm^3 molecule^{-1} s^{-1} [28], OH + neo-pentane 8.25×10^{-13} cm^3 molecule^{-1} s^{-1} [45]). As $k_{1,C\text{-}H}$ is slightly greater than the rate coefficient

for OH and neo-pentane, it does suggest, some activation of C-H abstraction, possibly via the formation of the pre-reactive complex (Figure 3). $k_{1,N\text{-}H}$ is significantly enhanced compared to N-H abstraction in methylamine for example, demonstrating the greater electron donating inductive effect of the *t*-butyl group.

The reaction of OH with piperazine is the most well studied reaction of OH with a diamine where the rate coefficient has been measured as 2.38×10^{-10} cm^3 molecule^{-1} s^{-1} in this group with C-H abstraction being the dominant pathway.[7] These fast kinetics and the predominance of C-H abstraction have been confirmed in two subsequent theoretical papers.[21, 46] However as a cyclic amine, with two secondary amine groups (generally faster kinetics than primary amines), this may not be the best comparator for N-methyl-1,3-propanediamine. An alternative comparison would be to consider N-methyl-1,3-propanediamine in a comparison with ethylamine and dimethylamine; the combination of these two rate coefficients, 2.54×10^{-11} cm^3 molecule^{-1} s^{-1} + 6.4×10^{-11} cm^3 molecule^{-1} s^{-1} = 8.94×10^{-11} cm^3 molecule^{-1} s^{-1} is in better agreement with our measured value of 7.09×10^{-11} cm^3 molecule^{-1} s^{-1}, which we believe to be a lower limit for the true rate coefficient.

A structure activity relationship (SAR) for nitrogen containing compounds has been developed by Borduas et al.[17] The SAR for several compounds from Borduas et al. are shown in Table 5. For the simpler amines there is good agreement with the overall rate coefficients, but poor agreement for N-H vs C-H branching ratios which are important in determining the fraction of nitramines and nitrosamines that can be formed during atmospheric oxidation. The SAR tends to over-predict abstraction from N-H and hence would over-predict nitramine and nitrosamine formation.

For *t*-butylamine there is poor agreement between the SAR (6.7×10^{-11} cm^3 molecule^{-1} s^{-1}) and the experimental determination of this work (1.7×10^{-11} cm^3 molecule^{-1} s^{-1}). Interestingly in this case, assuming the SAR prediction of 2.6×10^{-11} cm^3 molecule^{-1} s^{-1} for abstraction from the NH_2 group, the SAR would predict predominantly C-H abstraction in contrast to the experimental and theoretical work of this study.

For N-methyl-1,3-propanediamine, the SAR predicts 1.92×10^{-10} cm^3 molecule^{-1} s^{-1}, where close to half of this reactivity is predicted to be at the central CH_2 which is activated by the very substantial β substituent effect of the SAR, F(-CH_2N<) = 10, of the two amine groups.

Finally, for N-methylformamide ($CH_3NHC(O)H$) there is good agreement between experiment, calculations and SAR, both in terms of the absolute rate coefficient and in the approximate 50:50 branching ratio for abstraction at the CH_3 and –C(O)H positions, resulting in negligible abstraction from the N-H site.

Table 5 also includes the results of a SAR for amines presented in Nielsen et al.[3] and based on an earlier SAR of Kwok and Atkinson.[47] Here there is no β substituent factor increasing the predicted fraction of reaction occurring at the N-H site for several compounds, particularly the diamines. Nielsen et al. discuss the difficulties, evident in Table 5, in constructing an SAR for amine reactions where reactivity and site specificity will be influenced by the formation of pre-reactive complexes.

Table 5. Comparison of Experimental Rate Coefficients and Branching Ratios with SAR predictions by Borduas et al.[17] and Nielsen et al.[3]

Nitrogen Compound	Study (year)	Borduas et al. SAR k_{298}[a]	Nielsen et al. SAR k_{298}[a]	Exptl k_{298}[a]	Borduas et al. SAR ratio for N-H abstraction	Nielsen et al. SAR ratio for N-H abstraction	Exptl ratio for abstraction at N-H
CH_3NH_2	Onel et al.[5-6] (2013, 2014)	2.66	2.0	1.89	0.98	0.95	0.24
	Carl and Crowley[48] (1998)			1.73			
	Atkinson and Pitts[30] (1977)			2.2			
	Butkovskaya and Setser[49] (2016)			2.0			0.26
$CH_3CH_2NH_2$	Onel et al.[5-6] (2013, 2014)	3.15	2.61	2.54	0.83	0.73	<0.51
	Carl and Crowley[48] (1998)			2.37			
	Atkinson and Pitts[31] (1978)			2.77			
$(CH_3)_2NH$	Onel et al.[5-6] (2013, 2014)	6.3	6.4	6.39	0.98	0.97	0.41
	Carl and Crowley[48] (1998)			6.49			
	Atkinson and Pitts[31] (1978)			6.62			
	Butkovskaya and Setser[49] (2016)			5.20			0.34
	Lindley et al.[50] (1979)						0.37
t-$C_4H_9NH_2$	This work	6.7	1.95	1.66	0.39	0.97	0.87
	Tan et al.[20] (2018)			0.84			0.96
	Koch et al.[32] (1996)			1.2			
Piperazine	Onel et al.[7] (2014)	28.8	15.8	23.8	0.45	0.78	0.09
	Ren and da Silva[21] (2019)			24.0			0.01
	Sarma et al.[46] (2017)			28.6			0.07
N-methyl Propane diamine	This work	19.2	10.0	7.09	0.46	0.81	
$CH_3NHC(O)H$	This work	0.80	n/a	1.03	~0	n/a	~0
	Bunkan et al.[26] (2015)			0.57			~0
	Borduas et al.[25] (2015)			1.01			
	Solignac et al.[24] (2005)			0.86			

a - 10^{11} x k_{298}/cm^3 $molecule^{-1}$ s^{-1}

The current work and comparison of the SARs with site specific rate coefficients suggests that there is more work to be done in refining the SARs. Such work is of great importance; it is becoming clear that reactions of highly functionalized molecules (including amine and amide functionality) play important roles in the atmosphere.[51-53] Experimental determinations of site specific reactivity will be challenging and therefore a fully validated SAR would be of great benefit.

Supporting Information

Supporting information for this paper which is available on line contains information on the potential energy surface for reaction R4, the reaction of $(CH_3)_2CH_2CNH_2$ with O_2, and MESMER input files for reactions R1 and R4.

Acknowledgements

We acknowledge NERC funding via the Spheres Doctoral Training Programme for THS and via NCAS for MAB. DJM was supported by the Brazilian National Council for Scientific and Technological Development (CNPq, grant reference number 206527/2014-4). Preliminary experiments on OH and TBA were performed by undergraduate students Amy Peace and James Warman.

Email Addresses for Corresponding Authors

M.A.Blitz@leeds.ac.uk, P.W.Seakins@leeds.ac.uk

References

1. Luis, P., Use of monoethanolamine (MEA) for CO_2 capture in a global scenario: Consequences and alternatives. *Desalination* **2016,** *380*, 93-99.
2. Saeed, I. M.; Alaba, P.; Mazari, S. A.; Basirun, W. J.; Lee, V. S.; Sabzoi, N., Opportunities and challenges in the development of monoethanolamine and its blends for post-combustion CO_2 capture. *Int. J. Greenh. Gas Control* **2018,** *79*, 212-233.
3. Nielsen, C. J.; Herrmann, H.; Weller, C., Atmospheric chemistry and environmental impact of the use of amines in carbon capture and storage (CCS). *Chem. Soc. Rev.* **2012,** *41* (19), 6684-6704.
4. Onel, L.; Blitz, M. A.; Seakins, P. W., Direct determination of the rate coefficient for the reaction of OH radicals with monoethanol amine (MEA) from 296 to 510 K. *J. Phys. Chem. Lett.* **2012,** *3* (7), 853-856.
5. Onel, L.; Thonger, L.; Blitz, M. A.; Seakins, P. W.; Bunkan, A. J. C.; Solimannejad, M.; Nielsen, C. J., Gas-phase reactions of OH with methyl amines in the presence or absence of molecular oxygen. An experimental and theoretical study. *J. Phys. Chem. A* **2013,** *117* (41), 10736-10745.
6. Onel, L.; Blitz, M.; Dryden, M.; Thonger, L.; Seakins, P., Branching ratios in reactions of OH radicals with methylamine, dimethylamine, and ethylamine. *Environ. Sci. Technol.* **2014,** *48* (16), 9935-9942.

7. Onel, L.; Dryden, M.; Blitz, M. A.; Seakins, P. W., Atmospheric oxidation of piperazine by OH has a low potential to form carcinogenic compounds. *Environ. Sci. Technol. Lett.* **2014,** *1* (9), 367-371.
8. Onel, L.; Blitz, M. A.; Breen, J.; Rickardcd, A. R.; Seakins, P. W., Branching ratios for the reactions of OH with ethanol amines used in carbon capture and the potential impact on carcinogen formation in the emission plume from a carbon capture plant. *PCCP* **2015,** *17* (38), 25342-25353.
9. Zhu, L.; Mikoviny, T.; Morken, A. K.; Tan, W.; Wisthaler, A., A compact and easy-to-use mass spectrometer for online monitoring of amines in the flue gas of a post-combustion carbon capture plant. *Int. J. Greenh. Gas Control* **2018,** *78*, 349-353.
10. Wang, Y. W.; Yang, G.; Lu, Y. Q.; Liu, Y. L.; Chen, J. M.; Wang, L., Detection of gaseous dimethylamine using vocus proton-transfer-reaction time-of-flight mass spectrometry. *Atmos. Environ.* **2020,** *243*.
11. Mao, J. B.; Yu, F. Q.; Zhang, Y.; An, J. Y.; Wang, L.; Zheng, J.; Yao, L.; Luo, G.; Ma, W. C.; Yu, Q., et al., High-resolution modeling of gaseous methylamines over a polluted region in china: Source-dependent emissions and implications of spatial variations. *Atmos. Chem. Phys.* **2018,** *18* (11), 7933-7950.
12. Ge, X. L.; Wexler, A. S.; Clegg, S. L., Atmospheric amines - part i. A review. *Atmos. Environ.* **2011,** *45* (3), 524-546.
13. Barnes, I.; Solignac, G.; Mellouki, A.; Becker, K. H., Aspects of the atmospheric chemistry of amides. *Chemphyschem* **2010,** *11* (18), 3844-3857.
14. Cape, J. N.; Cornell, S. E.; Jickells, T. D.; Nemitz, E., Organic nitrogen in the atmosphere - where does it come from? A review of sources and methods. *Atmos. Res.* **2011,** *102* (1-2), 30-48.
15. Moller, K. H.; Berndt, T.; Kjaergaard, H. G., Atmospheric autoxidation of amines. *Environ. Sci. Technol.* **2020,** *54* (18), 11087-11099.
16. Glarborg, P.; Andreasen, C. S.; Hashemi, H.; Qian, R. C.; Marshall, P., Oxidation of methylamine. *Int. J. Chem. Kinet.* **2020,** *52* (12), 893-906.
17. Borduas, N.; Abbatt, J. P. D.; Murphy, J. G.; So, S.; da Silva, G., Gas-phase mechanisms of the reactions of reduced organic nitrogen compounds with OH radicals. *Environ. Sci. Technol.* **2016,** *50* (21), 11723-11734.
18. Speak, T. H.; Blitz, M. A.; Stone, D.; Seakins, P. W., A new instrument for time-resolved measurement of HO_2 radicals. *Atmos. Meas. Tech.* **2020,** *13* (2), 839-852.
19. Stone, D.; Blitz, M.; Ingham, T.; Onel, L.; Medeiros, D. J.; Seakins, P. W., An instrument to measure fast gas phase radical kinetics at high temperatures and pressures. *Rev. Sci. Instrum.* **2016,** *87* (5).
20. Tan, W.; Zhu, L.; Mikoviny, T.; Nielsen, C. J.; Wisthaler, A.; Eichler, P.; Muller, M.; D'Anna, B.; Farren, N. J.; Hamilton, J. F., et al., Theoretical and experimental study on the reaction of tert-butylamine with OH radicals in the atmosphere. *J. Phys. Chem. A* **2018,** *122* (18), 4470-4480.
21. Ren, Z. H.; da Silva, G., Atmospheric oxidation of piperazine initiated by OH: A theoretical kinetics investigation. *ACS Earth Space Chem.* **2019,** *3* (11), 2510-2516.
22. Almeida, J.; Schobesberger, S.; Kurten, A.; Ortega, I. K.; Kupiainen-Maatta, O.; Praplan, A. P.; Adamov, A.; Amorim, A.; Bianchi, F.; Breitenlechner, M., et al., Molecular understanding of sulphuric acid-amine particle nucleation in the atmosphere. *Nature* **2013,** *502* (7471), 359-364.
23. Koch, R.; Palm, W. U.; Zetzsch, C., First rate constants for reactions of OH radicals with amides. *Int. J. Chem. Kinet.* **1997,** *29* (2), 81-87.
24. Solignac, G.; Mellouki, A.; Le Bras, G.; Barnes, I.; Benter, T., Kinetics of the OH and Cl reactions with n-methylformaraide, N,N-dimethylformaraide and N,N-dimethylacetamide. *J. Photochem. Photobiol. A-Chem.* **2005,** *176* (1-3), 136-142.
25. Borduas, N.; da Silva, G.; Murphy, J. G.; Abbatt, J. P. D., Experimental and theoretical understanding of the gas phase oxidation of atmospheric amides with OH radicals: Kinetics, products, and mechanisms. *J. Phys. Chem. A* **2015,** *119* (19), 4298-4308.

26. Bunkan, A. J. C.; Hetzler, J.; Mikoviny, T.; Wisthaler, A.; Nielsen, C. J.; Olzmann, M., The reactions of n-methylformamide and N,N-dimethylformamide with OH and their photo-oxidation under atmospheric conditions: Experimental and theoretical studies. *PCCP* **2015,** *17* (10), 7046-7059.
27. Dunlop, J. R.; Tully, F. P., A kinetic-study of OH radical reactions with methane and perdeuterated methane. *J. Phys. Chem.* **1993,** *97* (43), 11148-11150.
28. Baasandorj, M.; Papanastasiou, D. K.; Talukdar, R. K.; Hasson, A. S.; Burkholder, J. B., $(CH_3)_3COOH$ (tert-butyl hydroperoxide): OH reaction rate coefficients between 206 and 375 K and the OH photolysis quantum yield at 248 nm. *PCCP* **2010,** *12* (38), 12101-12111.
29. Baeza-Romero, M. T.; Glowacki, D. R.; Blitz, M. A.; Heard, D. E.; Pilling, M. J.; Rickard, A. R.; Seakins, P. W., A combined experimental and theoretical study of the reaction between methylglyoxal and OH/OD radical: OH regeneration. *PCCP* **2007,** *9* (31), 4114-4128.
30. Atkinson, R.; Perry, R. A.; Pitts, J. N., Rate constants for reaction of OH radical with CH_3SH and CH_3NH_2 over temperature-range 299-426 K. *J. Chem. Phys.* **1977,** *66* (4), 1578-1581.
31. Atkinson, R.; Perry, R. A.; Pitts, J. N., Rate constants for reactions of OH radical with $(CH_3)_2NH$, $(CH_3)_3N$, and $C_2H_5NH_2$ over temperature-range 298-426 K. *J. Chem. Phys.* **1978,** *68* (4), 1850-1853.
32. Koch, R.; Kruger, H. U.; Elend, M.; Palm, W. U.; Zetzsch, C., Rate constants for the gas-phase reaction of OH with amines: Tert-butyl amine, 2,2,2-trifluoroethyl amine, and 1,4-diazabicyclo 2.2.2 octane. *Int. J. Chem. Kinet.* **1996,** *28* (11), 807-815.
33. Glowacki, D. R.; Liang, C. H.; Morley, C.; Pilling, M. J.; Robertson, S. H., Mesmer: An open-source master equation solver for multi-energy well reactions. *J. Phys. Chem. A* **2012,** *116* (38), 9545-9560.
34. Bartis, J. T.; Widom, B., Stochastic-models of interconversion of 3 or more chemical species. *J. Chem. Phys.* **1974,** *60* (9), 3474-3482.
35. Medeiros, D. J.; Blitz, M. A.; James, L.; Speak, T. H.; Seakins, P. W., Kinetics of the reaction of OH with isoprene over a wide range of temperature and pressure including direct observation of equilibrium with the OH adducts. *J. Phys. Chem. A* **2018,** *122* (37), 7239-7255.
36. Howes, N. U. M.; Lockhart, J. P. A.; Blitz, M. A.; Carr, S. A.; Baeza-Romero, M. T.; Heard, D. E.; Shannon, R. J.; Seakins, P. W.; Varga, T., Observation of a new channel, the production of CH_3, in the abstraction reaction of OH radicals with acetaldehyde. *PCCP* **2016,** *18* (38), 26423-26433.
37. Carr, S. A.; Baeza-Romero, M. T.; Blitz, M. A.; Pilling, M. J.; Heard, D. E.; Seakins, P. W., OH yields from the CH_3CO+O_2 reaction using an internal standard. *Chem. Phys. Lett.* **2007,** *445* (4-6), 108-112.
38. Blitz, M.; Pilling, M. J.; Robertson, S. H.; Seakins, P. W., Direct studies on the decomposition of the tert-butoxy radical and its reaction with NO. *PCCP* **1999,** *1* (1), 73-80.
39. Lazarou, Y. G.; Kambanis, K. G.; Papagiannakopoulos, P., Gas-phase reactions of $(CH_3)_2N$ radicals with NO and NO_2. *J. Phys. Chem.* **1994,** *98* (8), 2110-2115.
40. Voice, A. K.; Vevelstad, S. J.; Chen, X.; Nguyen, T.; Rochelle, G. T., Aqueous 3-(methylamino)propylamine for CO2 capture. *Int. J. Greenh. Gas Control* **2013,** *15*, 70-77.
41. Mouhoubi, S.; Dubois, L.; Loldrup Fosbøl, P.; De Weireld, G.; Thomas, D., Thermodynamic modeling of CO2 absorption in aqueous solutions of N,N-diethylethanolamine (deea) and n-methyl-1,3-propanediamine (mapa) and their mixtures for carbon capture process simulation. *Chemical Engineering Research and Design* **2020,** *158*, 46-63.
42. Daubert, T. E.; Danner, R. P., *Physical and thermodynamic properties of pure chemicals (data compilation)*. Hemisphere Publishing Corporation: New York, 1989.
43. Heinrich, J.; Ilovsky, J.; Surovy, J., Abhängigkeit des dampfdrucks des n-methylformamids von der temperatur. Flüssigkeit-dampf-gleichgewicht des systems n-methylformamid-wasser. *Chemicke Zvesti* **1961,** *15*, 414-418.
44. Sime, S. L.; Blitz, M. A.; Seakins, P. W., Rate coefficients for the reactions of OH with butanols from 298 K to temperatures relevant for low-temperature combustion. *Int. J. Chem. Kinet.* **2020,** *52* (12), 1046-1059.

45. Atkinson, R.; Baulch, D. L.; Cox, R. A.; Crowley, J. N.; Hampson, R. F.; Hynes, R. G.; Jenkin, M. E.; Rossi, M. J.; Troe, J., Evaluated kinetic and photochemical data for atmospheric chemistry: Volume ii - gas phase reactions of organic species. *Atmos. Chem. Phys.* **2006,** *6*, 3625-4055.
46. Sarma, P. J.; Gour, N. K.; Bhattacharjee, D.; Mishra, B. K.; Deka, R. C., Hydrogen atom abstraction from piperazine by hydroxyl radical: A theoretical investigation. *Mol. Phys.* **2017,** *115* (8), 962-970.
47. Kwok, E. S. C.; Atkinson, R., Estimation of hydroxyl radical reaction-rate constants for gas-phase organic-compounds using a structure-reactivity relationship - an update. *Atmos. Environ.* **1995,** *29* (14), 1685-1695.
48. Carl, S. A.; Crowley, J. N., Sequential two (blue) photon absorption by NO_2 in the presence of H_2 as a source of OH in pulsed photolysis kinetic studies: Rate constants for reaction of OH with CH_3NH_2, $(CH_3)_2NH$, $(CH_3)_3N$, and $C_2H_5NH_2$ at 295 K. *J. Phys. Chem. A* **1998,** *102* (42), 8131-8141.
49. Butkovskaya, N. I.; Setser, D. W., Branching ratios and vibrational distributions in water-forming reactions of OH and OD radicals with methylamines. *J. Phys. Chem. A* **2016,** *120* (34), 6698-6711.
50. Lindley, C. R. C.; Calvert, J. G.; Shaw, J. H., Rate studies of the reactions of the $(CH_3)_2N$ radical with O_2, NO, and NO_2. *Chem. Phys. Lett.* **1979,** *67* (1), 57-62.
51. Mutzel, A.; Poulain, L.; Berndt, T.; Iinuma, Y.; Rodigast, M.; Boge, O.; Richters, S.; Spindler, G.; Sipila, M.; Jokinen, T., et al., Highly oxidized multifunctional organic compounds observed in tropospheric particles: A field and laboratory study. *Environ. Sci. Technol.* **2015,** *49* (13), 7754-7761.
52. Schervish, M.; Donahue, N. M., Peroxy radical chemistry and the volatility basis set. *Atmos. Chem. Phys.* **2020,** *20* (2), 1183-1199.
53. Rissanen, M. P.; Kurten, T.; Sipila, M.; Thornton, J. A.; Kangasluoma, J.; Sarnela, N.; Junninen, H.; Jorgensen, S.; Schallhart, S.; Kajos, M. K., et al., The formation of highly oxidized multifunctional products in the ozonolysis of cyclohexene. *J. Am. Chem. Soc.* **2014,** *136* (44), 15596-15606.

TOC GRAPHIC

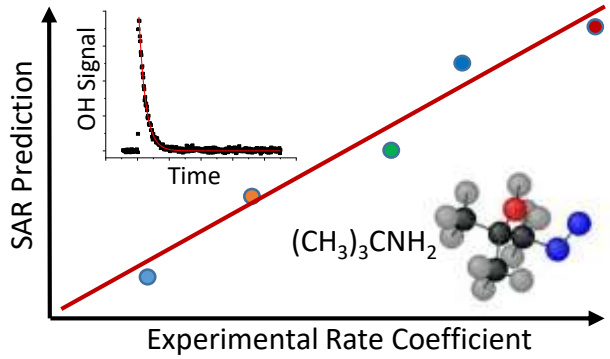
SAR Prediction
OH Signal
Time
$(CH_3)_3CNH_2$
Experimental Rate Coefficient